


 Cite this: *RSC Adv.*, 2023, **13**, 18090

# Fast-response photothermal bilayer actuator based on poly(*N*-isopropylacrylamide)–graphene oxide–hydroxyethyl methacrylate/polydimethylsiloxane†

 Shun Li,<sup>a</sup> Zhuo Cai,<sup>a</sup> Jiemin Han,<sup>a</sup> Yifei Ma,<sup>a</sup> \*<sup>a</sup> Zhaomin Tong,<sup>a</sup> Mei Wang,<sup>a</sup> \*<sup>a</sup> Liantuan Xiao,<sup>a</sup> Suotang Jia<sup>a</sup> and Xuyuan Chen<sup>ab</sup>

Demands for highly deformable and responsive intelligent actuators are increasing rapidly. Herein, a photothermal bilayer actuator consisting of a photothermal-responsive composite hydrogel layer and a polydimethylsiloxane (PDMS) layer is presented. The photothermal-responsive composite hydrogel is prepared by compositing hydroxyethyl methacrylate (HEMA) and the photothermal material graphene oxide (GO) with the thermal-responsive hydrogel poly(*N*-isopropylacrylamide) (PNIPAM). The HEMA improves the transport efficiency of water molecules inside the hydrogel network, eliciting a fast response and large deformation, facilitating greater bending behavior of the bilayer actuator, and improving the mechanical and tensile properties of the hydrogel. Moreover, GO enhances the mechanical properties and the photothermal conversion efficiency of the hydrogel in the thermal environment. This photothermal bilayer actuator can be driven under various conditions, such as hot solution, simulated sunlight, and laser, and can achieve large bending deformation with desirable tensile properties, broadening the application conditions for bilayer actuators, such as artificial muscles, bionic actuators, and soft robotics.

Received 15th May 2023

Accepted 9th June 2023

DOI: 10.1039/d3ra03213b

[rsc.li/rsc-advances](https://rsc.li/rsc-advances)

## Introduction

Hydrogel actuators are some of the most promising devices for smart materials with unique environmental response properties to temperature,<sup>1</sup> humidity,<sup>2</sup> pH,<sup>3,4</sup> light,<sup>5,6</sup> special chemicals,<sup>7</sup> magnetic fields,<sup>8</sup> electric fields,<sup>9</sup> *etc.* Hydrogel actuators have been at the forefront of intelligent hydrogel research and have shown promising applications in controllable switches, soft robots, wearable devices, artificial muscles, electronic skin,<sup>10–13</sup> *etc.* Hydrogel actuators can undergo prompt and reversible shape deformation in response to external stimuli,<sup>14</sup> which can induce mechanical motions including bending and twisting. Nonetheless, most hydrogel actuators are subject to harsh stimuli conditions and it is difficult to achieve fast and autonomous deformation. For example, a pH-stimulated actuator needs to repeatedly change the pH of the environment in order to perform actuation, making it challenging to actuate freely and automatically. In addition, although smart materials

produce corresponding stimulatory responses under different stimulation conditions, the response is weak and the shape transformation is usually inefficient to achieve fast actuation deformation, which greatly limits their applications in smart actuation fields such as biomedicine,<sup>15,16</sup> robotics<sup>17–19</sup> and microfluidics.<sup>20–22</sup>

To make the responses of the hydrogel actuators prompt and environment-adaptable, light-stimulated actuators are drawing enormous attention due to their advantage of remote controllability in comparison to other stimuli that require attaching cables or electrodes. Photoinduced deformation can be achieved by involving photothermal materials, such as graphene oxide (GO),<sup>23</sup> gold nanomaterials,<sup>24,25</sup> Fe<sub>3</sub>O<sub>4</sub> nanoparticles,<sup>26</sup> polypyrrole,<sup>27</sup> *etc.*, into the hydrogels, which can help the hydrogel actuators respond to visible or near-infrared radiation. Among them, GO exhibits light absorption in the visible and near-infrared wavebands and displays a notable photothermal conversion efficiency in the near-infrared band.<sup>28,29</sup> In addition to its favorable physical/chemical properties (*e.g.*, large surface area, extraordinary flexibility, mechanical strength, electrical and thermal conductivity, and excellent biocompatibility), GO shows great promise in manufacturing smart actuators. When GO is incorporated into a polymer matrix, it can convert absorbed near-infrared light into thermal energy, increasing the temperature of the nanocomposite. Moreover, GO can also act as a nano-crosslinker to enhance the mechanical properties of hydrogels.<sup>21,22,30,31</sup>

<sup>a</sup>State Key Laboratory of Quantum Optics and Quantum Optics Devices, Institute of Laser Spectroscopy, Collaborative Innovation Center of Extreme Optics, Shanxi University, Taiyuan 030006, China. E-mail: mayifei@sxu.edu.cn; wangmei@sxu.edu.cn

<sup>b</sup>Faculty of Technology, Natural Sciences and Maritime Sciences, Department of Microsystems, University of Southeast Norway, Borre N-3184, Norway

† Electronic supplementary information (ESI) available. See DOI: <https://doi.org/10.1039/d3ra03213b>



However, merely combining photothermal material with thermally responsive hydrogel only enhances the shrinkage deformation of the thermally responsive hydrogel itself under light radiation, but cannot achieve the practical functions such as bending. For example, Yu<sup>32</sup> *et al.* combined temperature-sensitive hydrogel, GO, and polyaniline (PANI) to prepare an infrared optical switch taking advantage of the photothermal shrinkage and electrical conductivity of the monolayer hydrogel. The switch of the circuit was controlled by controlling the contraction and expansion of the hydrogel. However, only when it shows more driving behaviors can it enrich its practical application. Nowadays, more and more research work is devoted to rational structural design, in which the construction of bilayer structures is an effective approach. The bilayer structure is composed of two layers with different coefficients of thermal expansion (CTE). Under light radiation, the active layer can convert light energy into thermal energy and conduct between the layers. Due to the different CTEs of the different active layers, the degree of thermal expansion/contraction under photothermal stimulation is different, and thus eventually the bilayer actuators will deviate towards the layer with the lower CTE, thus achieving the bending behavior. Lin<sup>33</sup> *et al.* affixed a thin layer of silicone rubber to a hydrogel layer to fabricate bilayer actuators which showed reversible and diverse bending/recovery behavior in response to temperature change of the water bath. Jiang<sup>34</sup> *et al.* prepared a temperature-triggered actuators with large scale movements in a short time using electrospun porous fibrous double layer membranes based on crosslinked thermo-responsive PNIPAM. Agarwal<sup>35,36</sup> *et al.* prepared a bilayer actuator with superfast reversible actuation by electrospinning. Although the bilayer structure gives the hydrogel actuator the ability to realize diverse driving behaviors, the lumpish structure leads to an excess burden on the whole actuator, probably resulting in poor actuation. Chen<sup>37</sup> *et al.* prepared a bilayer actuator driven by NIR light using temperature-sensitive hydrogel with GO, which is able to show bending and shape memory behavior, but it still needs further improvement on the bending angle and efficiency. Therefore, preparing highly responsive bilayer actuators with greater deformation capability is a great challenge at present.

Herein, we develop a photothermal bilayer actuator, which consists of a photothermal-responsive composite hydrogel layer and a PDMS layer. The photothermal-responsive composite hydrogel is prepared by combining HEMA and the photothermal GO with the thermal-responsive PNIPAM hydrogel. On the one hand, the HEMA improves the transport efficiency of water molecules inside the hydrogel network, providing a fast response and large deformation, facilitating greater bending behavior of the bilayer actuator, and improving the mechanical and tensile properties of the hydrogel. On the other hand, the GO enhances the mechanical properties and the photothermal conversion efficiency of the hydrogel at the thermal environment. This photothermal bilayer actuator can be driven under environmental conditions such as hot solution, simulated sunlight, and laser. Meanwhile, it can achieve large bending motion and desirable tensile properties, which broadens the

application areas of bilayer actuators such as artificial muscles, bionic actuators, and soft robotics.

## Experimental

### Preparation of the PNIPAM–GO–HEMA (PGH) composite hydrogel

The PGH composite hydrogel was obtained by free radical polymerization and curing. NIPAM (98%, Maclin Biochemical Technology Co., Ltd, Shanghai), GO (98.5%, Institute of Coal Chemistry, Chinese Academy of Sciences) nanopowders, HEMA (96%, Aladdin Reagent Co., Ltd, Shanghai), *N,N'*-methylenebis(acrylamide) (BIS, 99%, Aladdin Reagent Co., Ltd, Shanghai), ammonium peroxodisulfate (APS, 98%, Aladdin Reagent Co., Ltd, Shanghai) and *N,N,N',N'*-tetramethylethylenediamine (TEMED, 99%, Aladdin Reagent Co., Ltd, Shanghai) were used as the monomer, photothermal agent, additive, chemical cross-link, initiator and promoter, respectively. 120 mg of GO nanopowder was added to 40 mL of deionized water (DI water) and dispersed by ultrasonication to form a homogeneous GO dispersion with a concentration of 3 mg mL<sup>-1</sup>. 0.4 g of NIPAM was added into 3 mL of GO solution and stirred evenly. Thereafter, 0.001 g of BIS, 30 μL of HEMA, 0.008 mL of TEMED, and 0.004 g of APS were successively added into the solution and stirred until complete dissolution. The precursor solution was poured into a 3D-printed mold (15 mm × 3 mm × 0.5 mm) and encapsulated by covering a glass plate on the top.

### Preparation of the PGH/PDMS bilayer actuator

PGH/PDMS bilayer actuator was prepared by the layer-by-layer method. PDMS base liquid and curing agent were mixed in a 10 : 1 ratio and cured in an oven at 80 °C for 2 h. After curing, the bilayer actuator was cut into arbitrary sizes and submerged in DI water to rehydrate the composite hydrogel film. At room temperature (25 °C), the curing was observed to be from the layer of composite hydrogel towards the layer of PDMS, meanwhile, the composite hydrogel film was firmly bound to the PDMS. The samples including pure PNIPAM, PH, PGH-1, and PGH-2 were synthesized, where the PH represents the PNIPAM hydrogels containing HEMA, PGH-1 represents the PNIPAM hydrogels containing HEMA, and GO with the concentration of 1 mg mL<sup>-1</sup>, and PGH-2 represents the PNIPAM hydrogels containing HEMA and GO with a concentration of 2 mg mL<sup>-1</sup>.

### Characterization

Thermogravimetric analysis (TGA) was carried out by the TGA-2 (METTLER TOLEDO) at a heating rate of 10 °C min<sup>-1</sup> under an N<sub>2</sub> atmosphere. Mechanical properties at room temperature were tested by the ZQ-990B with a gauge length of 10 mm, at the loading rate of 0.5 mm min<sup>-1</sup>. The UV-Vis-NIR spectra of the composite hydrogel were measured with a UV-Vis-NIR spectrometer (LAMBDA 1050+, PerkinElmer). Xenon lamp light sources (780–2500 nm, MICROSOLAR300, Perfect Light; 250–2500 nm, MICROSOLAR300, Perfect Light) and the broadband



laser (SC-5-FC, YSL Photonics) were used for photothermal actuation.

## Results and discussion

As shown in Fig. 1a, in the PGH composite hydrogels, the NIPAM molecular chains become intertwined with the HEMA molecular chains and copolymerization takes place. The cross-linking agent BIS links the molecular chains of the NIPAM monomers. The photothermal material GO is linked to the amide group on NIPAM by hydrogen bonding. The persulphate in the initiator APS is thermally decomposed to generate anionic radicals to initiate polymerization in the hydrogel system. The promoter TEMED is used in conjunction with the APS to catalyze the generation of radicals from APS and to promote the polymerization reaction within the system, resulting in the formation of a three-dimensional mesh structure, thus forming a photothermally responsive PGH composite hydrogel. In order to study the effect of each component within the hydrogel layer on the driving effect, the properties of the PNIPAM-based hydrogels compounded with HEMA and GO are studied. In addition, as shown in Fig. 1b, the PGH/PDMS bilayer actuators are prepared by a facile and reproducible layer-by-layer method. First, the PGH precursor solution is filled into a 3D-printed PLA rectangular mold, and a glass plate is covered on the top to isolate oxygen. The PGH hydrogel films are prepared by free radical polymerization. After the composite hydrogel films are fully cured, remove the top glass cover, evenly

coat the PDMS mixture on the composite hydrogel films, shake the PDMS evenly with a shaker, and then cure the PDMS layer in an oven at 80 °C. During the PDMS curing, a filter paper, which is soaked with DI water, is put below the hydrogel for replenishing water. The filter paper is repeatedly moistened until the PDMS is fully cured. The bilayer actuator is finally cut even around the edges and placed in DI water to replenish water. To demonstrate the heat of curing at 80 °C has no effect on GO, XRD analysis of the GO is carried out, as shown in Fig. S1.† It can be seen that both the GO and GO heated at 80 °C for 2 h present peaks at around 12.5°, indicating that the GO is not reduced during the PDMS curing.

Thermogravimetric analysis (TGA) is carried out to study the effect of GO and HEMA introduced into the PNIPAM matrix on the thermal properties of hydrogels. As shown in Fig. 2a, it can be seen from the TGA curves that in Stage 1: at 0–160 °C, the drop in weight is mainly derived from the escape of absorbed water and the samples start to thermally degrade (thermal decomposition of the organic components in PNIPAM).<sup>37,38</sup> And around 100–120 °C, loss of water of crystallization and bound water happen. Stage 2: at 160–410 °C, thermal decomposition is completed and the mass gradually stabilizes. Stage 3: at 410–600 °C, weight loss occurs due to the degradation of the PNIPAM backbone. The results indicate that the introduction of GO nanoparticles and HEMA polymers had little effect on the main thermal performance trends of the PNIPAM matrix hydrogels. From the DTG curves in Fig. 2b, it can be seen that the rate of

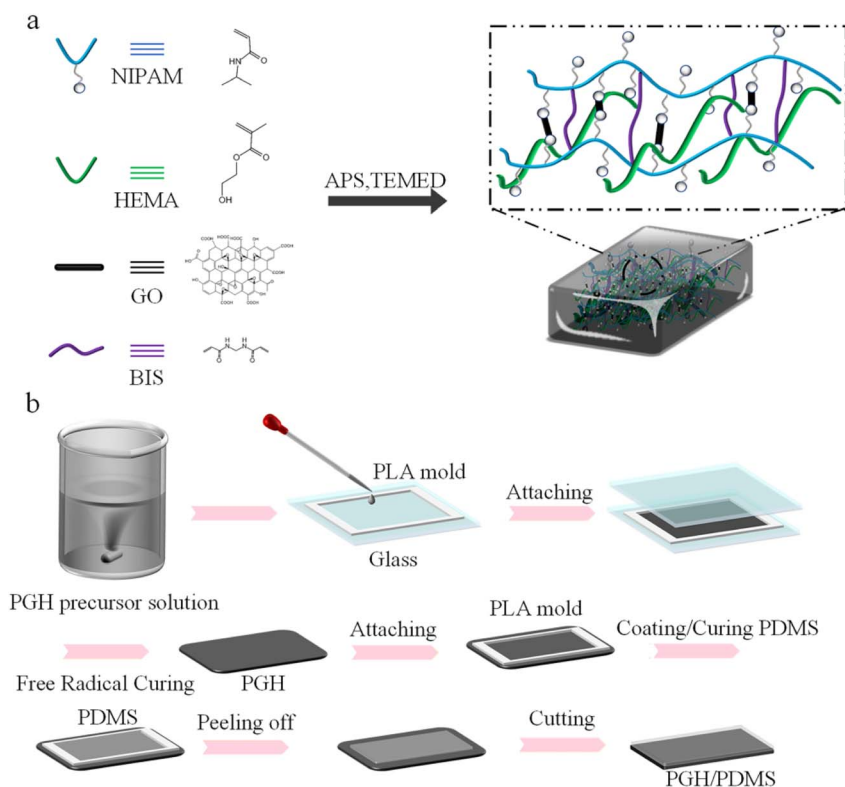


Fig. 1 (a) Schematic illustration for the preparation of PNIPAM-based composite hydrogel. (b) Schematic illustration of the preparation process of the PGH/PDMS photothermal bilayer actuator.



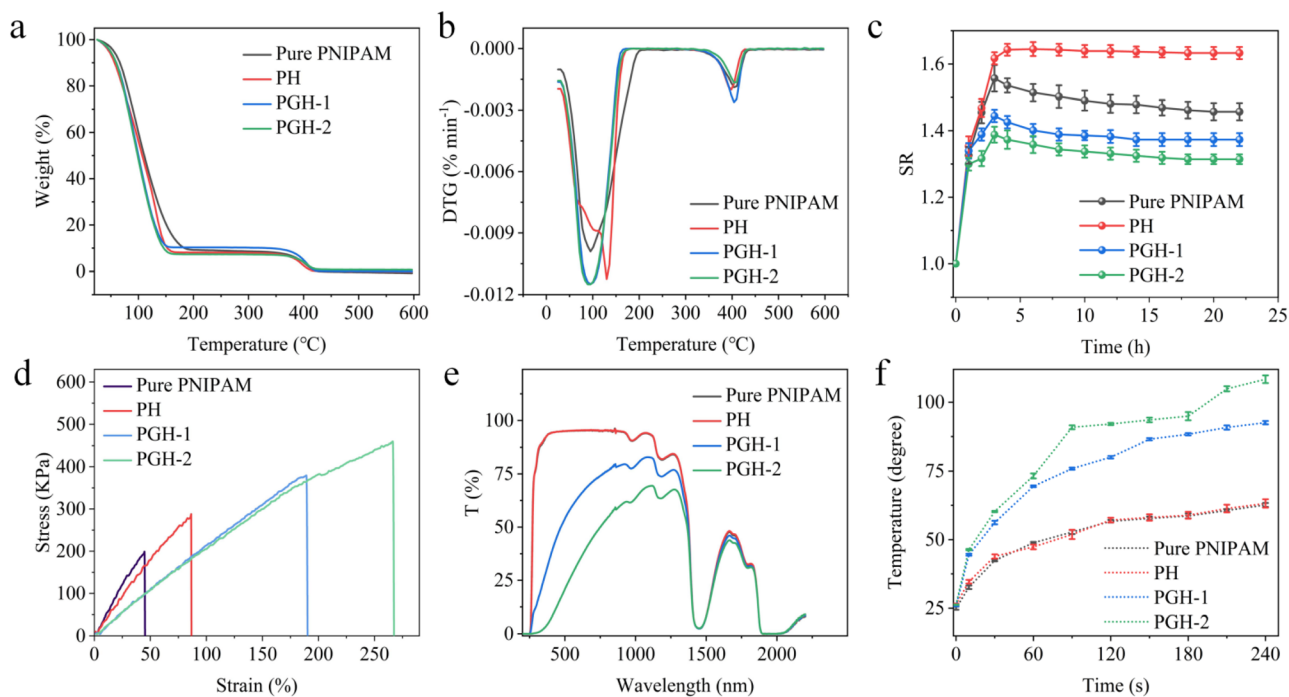


Fig. 2 Characterizations of PNIPAM-based composite hydrogel films. (a) TGA curves of PNIPAM-based hydrogel films. (b) DTG curves of PNIPAM-based hydrogel films. (c) The swelling ratio (SR) of PNIPAM-based hydrogel films. (d) Strain–stress curves of PNIPAM-based hydrogel films in air. (e) UV-Vis-NIR spectra of PNIPAM-based hydrogel films. (f) The temperature change of PNIPAM-based hydrogel films under the illumination of a xenon lamp.

thermal decomposition increases with the addition of HEMA, demonstrating that the addition of HEMA enhances the transport efficiency of water molecules within the hydrogel network and thus allows the composite hydrogels to have a faster thermal decomposition rate and response to heat more rapidly. The thermal decomposition rate also increases with the addition of GO. According to the theory of Lake and Thomas 1967,<sup>39</sup> the efficiency of water molecule transport inside the hydrogel network is inversely proportional to the square of the cross-link density, and excessive cross-link density decreases the efficiency of water molecule transport inside the hydrogel network. In our PGH hydrogel, GO is hydrogen-bonded in the polymer and acts as a nano-crosslinker, enhancing the degree of a cross-link of the network but decreasing the efficiency of water molecule transport inside the hydrogel network, thus weakening the thermal decomposition rate of the composite hydrogels. However, an increase in the thermal decomposition rate is observed in Fig. 2b, which is due to the enhancement of the thermal conductivity derived from GO.

In order to study the water absorption properties of different PNIPAM-based hydrogel films, the swelling ratio of the hydrogel films in DI water is also investigated. According to the equation:

$$SR = m_t/m_0$$

The  $m_t$  is the mass of the hydrogel films and the  $m_0$  is the initial mass of the hydrogel films. As shown in Fig. 2c, the pure PNIPAM hydrogel is found to exhibit a high swelling ratio (1.56)

in DI aqueous solution, which is because the pure PNIPAM hydrogel at room temperature behaves hydrophilic in an aqueous environment and swells with water absorption. The HEMA contains hydrophilic hydroxyl groups. When the HEMA is added to the hydrogel, the NIPAM molecular chains become intertwined with the HEMA molecular chains, increasing the transport efficiency of the water molecules within the hydrogel network, and resulting in an increase in the swelling ratio (1.59). In addition, when the GO concentration is 1 mg mL<sup>-1</sup>, a significant decrease in the swelling ratio (1.38) of the PGH-1 occurs. As the GO content increases, the swelling ratio (1.32) of the PGH-2 also decreases when the GO concentration reaches 2 mg mL<sup>-1</sup>, due to rich oxygen-containing functional groups in GO, such as epoxy groups, carboxylic groups, and hydroxyl groups, which provide abundant active centers for the formation of hydrogen bonds.<sup>40</sup> Hence, the amide groups in PNIPAM can be connected to GO *via* hydrogen bonds,<sup>41,42</sup> linking the hydrogel network more tightly, thereby weakening the water transportation inside the hydrogel. As a result, the PGH-2 presents a decrease in the swelling rate.

Excellent mechanical properties can broaden the application fields of hydrogel, while the tensile strain (44.6%) of pure PNIPAM is poor and the tensile stress (199.3 kPa) is low, which greatly limits its application. As been reported, to improve the mechanical properties of PNIPAM hydrogel, the most commonly used method is to improve the network structure of hydrogel or add nanoparticles.<sup>24–26</sup> Compared with the reported hydrogel actuators, our strategy endows the composite hydrogels with higher mechanical strength through the cooperation



of HEMA and GO in the hydrogel network. To evaluate the mechanical properties of the composite hydrogels, the stress-strain curves are measured as shown in Fig. 2d. The tensile strain (86.4%) and tensile stress (288.0 kPa) of the PH are improved compared with pure PNIPAM due to the cross-linking of the HEMA and PNIPAM, which strengthens the internal network structure of the composite hydrogels and enhances its mechanical properties. Additionally, with the addition of GO nano-filler, the tensile strain (189.6%) and tensile stress (380.2 kPa) of the PGH-1 is further improved, because the GO, as a nano-crosslinker, is connected to the PNIPAM by forming hydrogen bonds. The GO nanosheets connect the internal network structure of the composite hydrogels more closely, reducing the voids of the hydrogel network, and thus having a key impact on the mechanical properties of the hydrogels. The mechanical properties of the PGH can be further enhanced by increasing the concentration of GO. The PGH-2 achieves a higher tensile strain (266.3%) and stronger tensile stress (459.6 kPa), which is 230% higher than that of pure PNIPAM.

The UV-Vis-NIR characterization is conducted to study the roles of HEMA and GO components on the chemical structure of the PNIPAM-based hydrogel films. As shown in Fig. 2e, the transmittance curve of the PH hydrogel coincides perfectly with that of pure PNIPAM when only HEMA is added, demonstrating that the HEMA has no impact on the transmittance. When the GO is added, the transmittance of the PGH composite hydrogels decreases obviously, proving that the addition of GO improves the light absorption of the hydrogels in the visible and near-infrared waveband. Additionally, as the GO concentration increases, the transmittance of the PGH composite hydrogels continues to decline, which proves that GO plays a positive role in improving the light absorption of the PGH hydrogels. As shown in Fig. S2,† the PNIPAM and PH hydrogels are transparent, while the PGH-1 and PGH-2 hydrogels are nearly black due to the high light absorption of GO. The hydrogel turns to brown color when cut into hydrogel films.

It has been reported that the PNIPAM hydrogel is a temperature-sensitive intelligent hydrogel with excellent temperature response.<sup>43–45</sup> GO has excellent light absorption properties and excellent photothermal conversion efficiency in visible light, especially in the near-infrared region, which can convert the absorbed light radiation energy into thermal energy when added to the polymer matrix. In our study, the wide band absorption and photothermal conversion properties of the hydrogels are investigated using a  $1.2 \text{ W cm}^{-2}$  xenon lamp light source (320–2500 nm) to confirm the improvement in the photothermal conversion performance by adding GO. As shown in Fig. 2f, the temperature response of pure PNIPAM and PH is obviously lower than that of the PGH composite hydrogels. The temperature of the PGH-1 can reach 92 °C after being exposed to the light for 4 min, and the temperature of the PGH-2 can rise to 107 °C with the increase in GO concentration, whereas the PNIPAM and PH can only reach about 62 °C. It can be seen that the GO nano-fillers play a significant role in enhancing the photothermal properties and thermal conductivity of the composite hydrogels.

Since the PGH composite hydrogel provides efficient light-induced volume contraction with raising temperature, a photo-thermal bilayer actuator is designed. This bilayer actuator is built using PDMS and PNIPAM-based composite hydrogel layers. Due to the CTE mismatch between the hydrogel and the PDMS as well as the strong adhesion between the two layers, the two layers show a large volume difference under photothermal stimulation, thus causing the bending of the actuator. The PNIPAM possesses both a highly hydrophobic polymethylene backbone and slightly hydrophobic isopropyl groups.<sup>46,47</sup> When the temperature is below the lower critical solution temperature (LCST) of the PNIPAM (32 °C), due to the hydrogen bonding between amide groups and water molecules in the hydrogel system, water molecules around the macromolecular chain form a highly ordered solvated shell connected by hydrogen bonds, the hydrogel exhibits hydrophilic. While with the increase in temperature, hydrophobic interaction within and between molecules is strengthened, forming a hydrophobic layer and destroying hydrogen bonds and the solvated shell around macromolecular chains. Therefore, at the temperature above the LCST of the PNIPAM, the hydrogel will change from hydrophilic to hydrophobic and water molecules are expelled from the hydrogel, thereby leading to volume shrinkage and exhibiting temperature-sensitive properties,<sup>42</sup> as presented in Fig. S3.† On the contrary, the PDMS undergoes thermal expansion as the temperature increases due to its high CTE value ( $3 \times 10^{-4} \text{ K}^{-1}$ ).

As shown in Fig. 3a, the reversible bending behavior of the PGH/PDMS photothermal bilayer actuator upon different conditions is illustrated. At room temperature, the bilayer actuators bend from the PGH layer to the PDMS layer because the PGH behaves hydrophilic in an aqueous environment when the temperature is lower than its LCST. As a result, it absorbs water and expands, causing the PGH layer to bend toward the PDMS layer. And the state at this point is defined as the equilibrium state. As shown in Fig. 3b and c, the bending change of

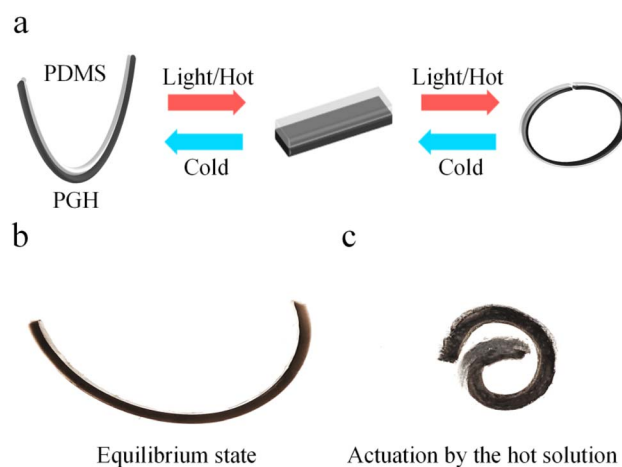


Fig. 3 Driving behavior of the PGH/PDMS photothermal bilayer actuator. (a) Schematic illustration of the reversible bending behavior of the PGH/PDMS photothermal bilayer actuator. (b and c) Digital photos of the bending change of the bilayer actuator in a hot solution.



the bilayer actuator in a hot solution is remarkable. The PDMS layer bends and deforms quickly toward the PGH side when the bilayer actuator is placed in a hot solution environment at 40 °C ( $T > LCST$ ), which is the exact opposite of the bending direction in the equilibrium state due to the difference in CTE between the two different active layers and the larger contraction of the PGH active layer. When the bilayer actuator is taken out from the hot solution, we can see that its bending behavior gradually returns to its equilibrium condition. And the generated bending behavior in this environment is completely reversible and reproducible.

The bending angle change ( $\Delta\theta$ ) of the bilayer actuator can represent the nature of the actuator. A desirable actuator can react quickly and exhibit a large  $\Delta\theta$  in a given environment. It is worth noting that the bilayer actuator bends in the negative direction at the equilibrium state at room temperature. Therefore, the bending of the PGH layer to the PDMS layer is defined as the negative angle  $\theta_1$ , while the bending of the PDMS to PGH layer is defined as the positive angle  $\theta_2$ , and the bending angle change  $\Delta\theta = \theta_2 - \theta_1$ . To study the impact of GO concentration in PGH films on the  $\Delta\theta$  of the bilayer actuator, the bilayer actuators with GO concentrations of 0, 1, and 2 mg mL<sup>-1</sup> are prepared in a 0.5 mm thickness of the hydrogel layer. As shown in Fig. 4a, the PH/PDMS bilayer actuator has a greater  $\Delta\theta$  than the PNIPAM/PDMS. A high response rate can be achieved by increasing the porosity of the internal network structure of hydrogel and decreasing the transmission resistance.<sup>48</sup> In addition, improving the hydrogel network structure can achieve

a faster response, a greater degree of bending deformation, and a higher tensile rate.<sup>49,50</sup> In this study, the crosslinking of the hydrophilic HEMA monomer with the PNIPAM during the free radical polymerization process results in a linear copolymer. The entanglement and hydrogen bonds between the HEMA and PNIPAM enable fast water transport. When the GO is added to the hydrogel (PGH-1/PDMS), a significant increase in the  $\Delta\theta$  (181°) is observed, which is nearly 6 times larger compared to that of the PNIPAM/PDMS (31°). Additionally, as the GO concentration increases, the  $\Delta\theta$  of the bilayer actuator of the PGH-2/PDMS (342°) increases approximately 11 times in comparison to that of the PNIPAM/PDMS due to the excellent heat transfer properties imparted by the uniformly dispersed GO. As the GO content increases, the heat transfer between the layers is enhanced. Thus, the bilayer actuator displays stronger bending behavior as a result of the larger difference in volume changes between the PGH and PDMS layers due to the different CTE. Although the volume change in the composite hydrogel is theoretically greater with higher GO concentration, if GO aggregates in the hydrogel matrix beyond the critical concentration, it will disturb the molecular chain structure of the hydrogel, leading to the failure of curing of the PGH hydrogel.

To demonstrate the effect of the hydrogel thickness on the bending property of the bilayer actuator, we fix the GO concentration in the hydrogel layer at 2 mg mL<sup>-1</sup> and prepare the bilayer actuator with the hydrogel layer thicknesses of 0.5 mm, 1.0 mm, and 1.5 mm (as indicated by the subscript in Fig. 4b), respectively. Meanwhile, the thickness of the PDMS

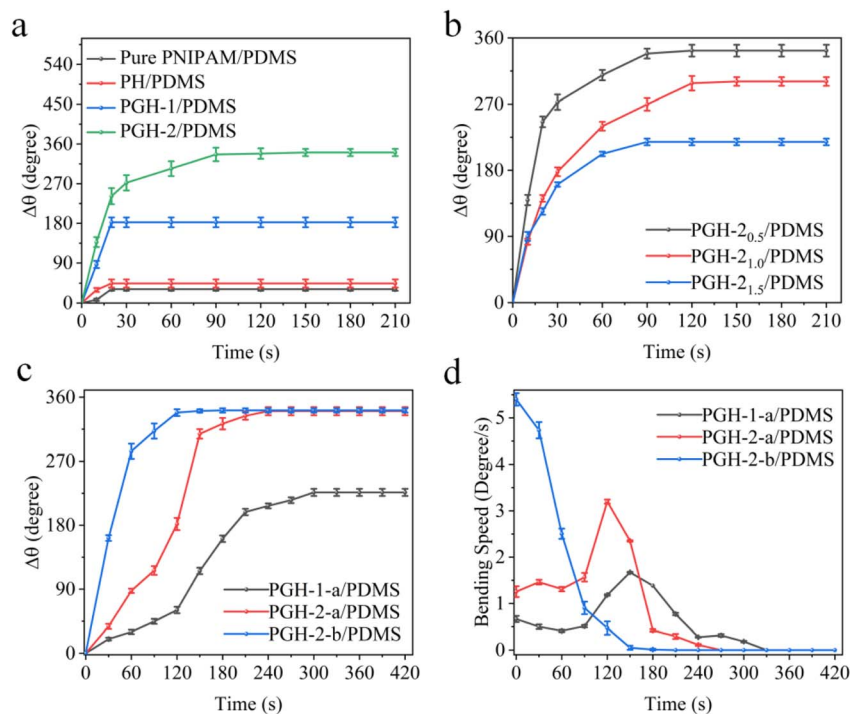


Fig. 4 Characterizations of thermo-/photothermal-responsive actuation behavior of the PNIPAM-based hydrogel/PDMS bilayer actuators. (a) The changing angle of the PNIPAM-based hydrogel/PDMS bilayer actuators under 40 °C water. (b) The changing angle of the bilayer actuators with different thicknesses of PGH-2 films under 40 °C water. (c) The changing angle of the PGH bilayer actuators under different illumination conditions. (d) The velocity of the changing angle of the PGH bilayer actuators under different illumination conditions.

layer maintains the same. As shown in Fig. 4b, the  $\Delta\theta$  of the bilayer actuator decreases as the thickness of the hydrogel layer increases. This is due to the increased volume ratio of the hydrogel to PDMS, weakening the actuation effect, which is not conducive to obtaining a bilayer actuator with desirable actuation performance. Moreover, for the bilayer actuator with a thicker hydrogel layer, water molecules require more time to diffuse from it, thus weakening the actuation velocity. Additionally, the effects of various hydrogel thicknesses on the bending angle change of the bilayer actuator with different GO concentrations are compared in Fig. S4,† wherein the hydrogel film with a GO concentration of  $2 \text{ mg mL}^{-1}$  and thickness of 0.5 mm shows the highest bending angle change.

Owing to the near-infrared photothermal effect and broadband absorption property of GO, light sources can be employed to drive the bilayer actuator. In order to explore the driving effect of the bilayer actuator in different wavelength ranges, a xenon lamp (lamp a, power density of  $1.2 \text{ W cm}^{-2}$ , 320–780 nm) is used to simulate visible light to drive the actuator. With exposure to the light source, the temperature of the photothermal bilayer actuator will rise, thereby actuating the bilayer film. As presented in Fig. 4c, when the bilayer actuator in the equilibrium state is exposed to the xenon lamp, the tendency of bending angle change of the PGH-1 and PGH-2 as time is consistent with the driving bending in the hot solution environment, that is, the bilayer actuator with a higher GO concentration exhibits a larger bending angle change. The changing angle of the PGH-2/PDMS bilayer actuator ( $342^\circ$ ) under xenon lamp a is significantly higher than that of PGH-1/PDMS ( $227^\circ$ ). Fig. 4d also demonstrates that the PGH-2 takes less time (120 s) than PGH-1 (150 s) to attain its maximum bending rate, and the bending rate is higher at this point. It can be found that the optical radiation driving of the bilayer actuator benefits from the increase in GO content in the hydrogel system. When the GO concentration increases, more GO sheets are connected by hydrogen bonding within the hydrogel system, so the actuator can warm up rapidly when affected by photothermal radiation, promoting the volume shrinkage deformation of PGH hydrogel and the driving deformation of PGH/PDMS bilayer actuator. In addition, another xenon lamp (lamp b, power density of  $1.2 \text{ W cm}^{-2}$ , 320–2500 nm) is utilized to drive the bilayer actuator. When the bilayer actuator in an equilibrium state is under illumination, the PGH-2-b/PDMS bilayer actuator reaches the same maximum bending angle change of  $342^\circ$ , but responds faster (120 s) compared to the actuator illuminated by xenon lamp a. This demonstrates that the bilayer actuator has significant light absorption and photothermal conversion properties for the broadband wavelength due to the near-infrared photothermal effect and broadband absorption properties of GO. Due to the strong absorption of GO in the region of 1200–2500 nm (Fig. 2e), the PGH-2-b/PDMS bilayer actuator can produce heat more quickly under the irradiation of lamp b,<sup>37,51,52</sup> resulting in rapid warming and promoting volume shrinkage deformation of the PGH hydrogel and driven deformation of the PGH/PDMS bilayer actuator.

As shown in Fig. 5a and b, the actuator bends from the PDMS side to the PGH hydrogel side under xenon lamp irradiation.

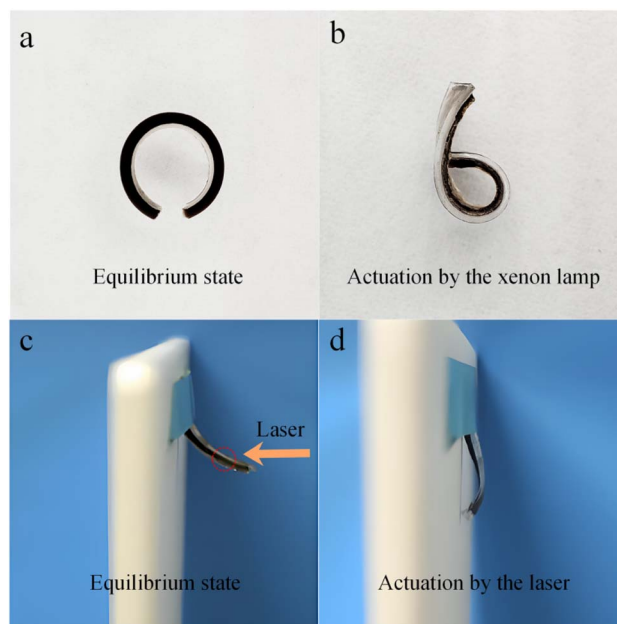


Fig. 5 Digital photos of the bending change of the PGH/PDMS photothermal bilayer actuator. (a and b) Under xenon lamp irradiation. (c and d) Under a broadband laser (320–2500 nm, 500 mW).

Unlike driving in hot solution, for one thing, the continuous photothermal radiation causes the PGH hydrogel to lose a significant amount of water by evaporation, leading to a drastic shrinkage of the PGH hydrogel. For another, the PDMS expands in volume through heat accumulation. Hence, the thickness of the PGH and PDMS of the actuator differs considerably before and after actuation. And impressively, the consistent maximum bending angle of PGH-2 under different light sources indicates that the wavebands have no impact on the maximum bending angle.

In addition to being driven in the hot solution and solar illumination, as shown in Fig. 5c and d, the PGH/PDMS bilayer actuator can also be driven by a broadband laser (320–2500 nm, 500 mW). The laser point size is set to 3–4 mm, and the PGH/PDMS bilayer actuator is placed 4 cm away from the light source. Polyimide tape is used to fix the PGH/PDMS bilayer actuator to the light shielding plate, and the initial state is shown in Fig. 5c. The central point of the PGH/PDMS bilayer actuator is continuously and intensively irradiated by laser in the air atmosphere at ambient temperature. Under the laser radiation, the actuator bends from the PDMS side to the PGH hydrogel side, as shown in Fig. 5d. It suggests that the bilayer actuator composed of PGH/PDMS in this study can be driven by hot solution, solar radiation, and laser radiation.

Finally, a “Y” shaped PGH/PDMS bilayer actuator is prepared and a broadband laser is used to irradiate the fixed target spot of the “Y” actuator vertically from top to bottom with a spot size of 3 mm. It is worth noting that, in Fig. 6a–d, the actuator is stimulated by localized photothermal radiation and a gradual bending of the upper part of the irradiated position can be observed. And as the laser irradiation time increases, the bending angle of the upper part of the “Y” actuator became larger and more palpable, while no significant stimulus-responsive deformation is observed in the



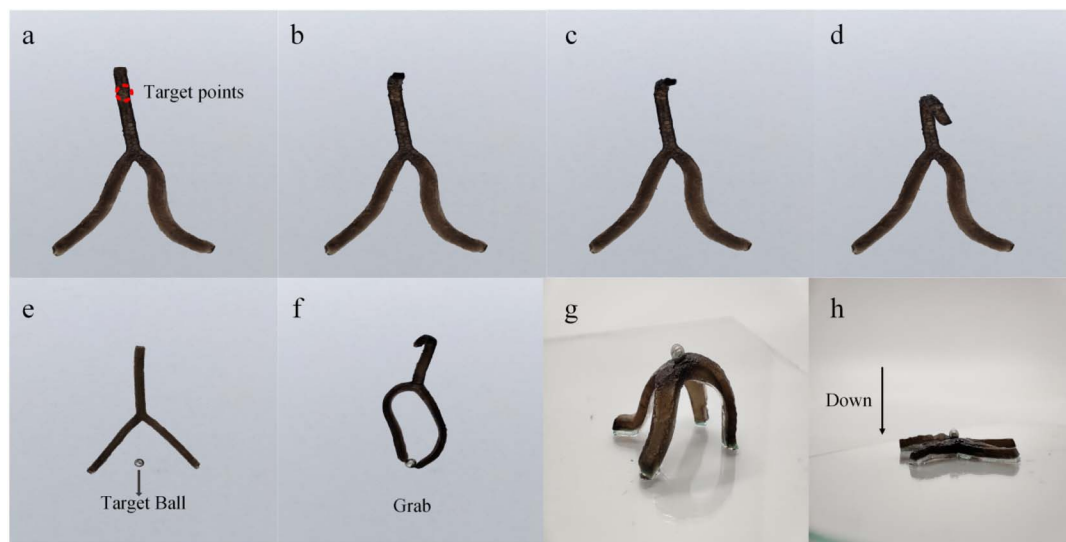


Fig. 6 (a–d) Independent driving behavior of the “Y” shaped actuator under local irradiation. (e and f) The driving behavior of the “Y” shaped actuator to capture a target ball. (g and h) The driving behavior of the “cross” shaped actuator to transport the target ball downward.

other parts that are not exposed to photothermal radiation, indicating that the actuator is capable of independent driving. In addition, in Fig. 6e and f, the two “arms” of the “Y” actuator are placed close to a target ball and then the actuator is stimulated by a hot solution, the actuator conducts a continuous bending behavior and finally captures the target ball, similar to the mechanical claws of a pinball machine. In Fig. 6g and f, a “cross” actuator is prepared, in which the PGH composite hydrogel bends and turns to the PDMS side in its natural state. By placing the target ball on top of the “spine” of the actuator and applying thermal stimulation to the actuator, thermal response deformation occurs. At this time, the PGH composite hydrogel contracts, and the PDMS side moves upwards, causing the center of gravity of the “cross” actuator to shift downwards, achieving vertical downward transport of the ball. Due to the strong adhesion of the PGH composite hydrogel itself, the target ball is not easily dislodged and is in good contact with the actuator throughout the transport process.

## Conclusions

In summary, a photothermal bilayer actuator consisting of a PGH photothermal-responsive hydrogel layer and PDMS layer has been successfully prepared, which can be driven under different conditions, including hot solution, simulated sunlight, and laser. In the hydrogel layer, by adding the appropriate amount of HEMA, the swelling rate and mechanical and tensile properties of the hydrogel are improved, facilitating the realization of greater bending behavior of the bilayer actuators. Furthermore, the addition of GO enhances the mechanical properties and photothermal conversion efficiency of the hydrogel under photothermal environment. The bending angle change as well as the actuation rate are significantly enhanced with increasing GO concentration, as a result, the PGH-2<sub>0.5</sub>/PDMS bilayer actuator achieves the maximum bending angle change (342°) within 90 s. The PGH/PDMS actuators show great

promise in artificial muscles, bionic actuators, and soft robotics, which also pave the path for the design and manufacture of novel intelligent systems.

## Author contributions

Conceptualization, Yifei Ma and Mei Wang; data curation, Shun Li; formal analysis, Shun Li, Jiemin Han and Zhuo Cai; funding acquisition, Yifei Ma, Mei Wang, Liantuan Xiao and Suotang Jia; supervision, Yifei Ma, Mei Wang, Liantuan Xiao, Suotang Jia and Xuyuan Chen; writing – original draft, Shun Li; writing – review & editing, Mei Wang, Yifei Ma, Liantuan Xiao, Suotang Jia and Xuyuan Chen.

## Conflicts of interest

There are no conflicts to declare.

## Acknowledgements

This research was supported by the National Key Research and Development Program of China (Grant 2022YFA1404001), the National Natural Science Foundation of China (Grants 21805174 and 51902190), the Key Research and Development Program of Shanxi Province for International Cooperation (201803D421082), the Research Project supported by Shanxi Scholarship Council of China (2021-004 and 2022-013), the 111 Project (Grant D18001), the Changjiang Scholars and Innovative Research Team in University of Ministry of Education of China (Grant IRT\_17R70), and the Fund for Shanxi “1331 Project”.

## Notes and references

- 1 J. Kim, J. A. Hanna, M. Byun, C. D. Santangelo and R. C. Hayward, *Science*, 2012, **335**, 1201–1205.



- 2 Y. Ma, Y. Zhang, B. Wu, W. Sun, Z. Li and J. Sun, *Angew. Chem., Int. Ed.*, 2011, **50**, 6254–6257.
- 3 Z. Han, P. Wang, G. Mao, T. Yin, D. Zhong, B. Yiming, X. Hu, Z. Jia, G. Nian, S. Qu and W. Yang, *ACS Appl. Mater. Interfaces*, 2020, **12**, 12010–12017.
- 4 Y. Zhang, J. Liao, T. Wang, W. Sun and Z. Tong, *Adv. Funct. Mater.*, 2018, **28**, 1707245.
- 5 C. Ma, W. Lu, X. Yang, J. He, X. Le, L. Wang, J. Zhang, M. J. Serpe, Y. Huang and T. Chen, *Adv. Funct. Mater.*, 2018, **28**, 1704568.
- 6 L. Zhang, X. Qiu, Y. Yuan and T. Zhang, *ACS Appl. Mater. Interfaces*, 2017, **9**, 41599–41606.
- 7 L. Zhao, J. Huang, Y. Zhang, T. Wang, W. Sun and Z. Tong, *ACS Appl. Mater. Interfaces*, 2017, **9**, 11866–11873.
- 8 Y. Kim, H. Yuk, R. Zhao, S. A. Chester and X. Zhao, *Nature*, 2018, **558**, 274–279.
- 9 D. Han, C. Farino, C. Yang, T. Scott, D. Browe, W. Choi, J. W. Freeman and H. Lee, *ACS Appl. Mater. Interfaces*, 2018, **10**, 17512–17518.
- 10 X. Qian, Y. Zhao, Y. Alsaïd, X. Wang, M. Hua, T. Galy, H. Gopalakrishna, Y. Yang, J. Cui, N. Liu, M. Marszewski, L. Pilon, H. Jiang and X. He, *Nat. Nanotechnol.*, 2019, **14**, 1048–1055.
- 11 H. Yuk, S. Lin, C. Ma, M. Takaffoli, N. X. Fang and X. Zhao, *Nat. Commun.*, 2017, **8**, 14230.
- 12 S. Xiao, M. Zhang, X. He, L. Huang, Y. Zhang, B. Ren, M. Zhong, Y. Chang, J. Yang and J. Zheng, *ACS Appl. Mater. Interfaces*, 2018, **10**, 21642–21653.
- 13 Z. Sun, Y. Yamauchi, F. Araoka, Y. S. Kim, J. Bergueiro, Y. Ishida, Y. Ebina, T. Sasaki, T. Hikima and T. Aida, *Angew. Chem., Int. Ed.*, 2018, **130**, 15998–16002.
- 14 S. J. Jeon, A. W. Hauser and R. C. Hayward, *Acc. Chem. Res.*, 2017, **50**, 161–169.
- 15 T. Hoare, B. P. Timko, J. Santamaria, G. F. Goya, S. Irusta, S. Lau, C. F. Stefanescu, D. Lin, R. Langer and D. S. Kohane, *Nano Lett.*, 2011, **11**, 1395–1400.
- 16 T. Y. Liu, S. H. Hu, T. Y. Liu, D. M. Liu and S. Y. Chen, *Langmuir*, 2006, **22**, 5974–5978.
- 17 N. Bassik, B. T. Abebe, K. E. Laflin and D. H. Gracias, *Polymer*, 2010, **51**, 6093–6098.
- 18 W. J. Zheng, N. An, J. H. Yang, J. Zhou and Y. M. Chen, *ACS Appl. Mater. Interfaces*, 2015, **7**, 1758–1764.
- 19 Z. Hu, X. Zhang and Y. Li, *Science*, 1995, **269**, 525–527.
- 20 S. R. Sershen, G. A. Mensing, M. Ng, N. J. Halas, D. J. Beebe and J. L. West, *Adv. Mater.*, 2005, **17**, 1366–1368.
- 21 C.-W. Lo, D. Zhu and H. Jiang, *Soft Matter*, 2011, **7**, 5604–5609.
- 22 C.-H. Zhu, Y. Lu, J. Peng, J.-F. Chen and S.-H. Yu, *Adv. Funct. Mater.*, 2012, **22**, 4017–4022.
- 23 X. He, Y. Sun, J. Wu, Y. Wang, F. Chen, P. Fan, M. Zhong, S. Xiao, D. Zhang, J. Yang and J. Zheng, *J. Mater. Chem. C*, 2019, **7**, 4970–4980.
- 24 Q. Shi, H. Xia, P. Li, Y.-S. Wang, L. Wang, S.-X. Li, G. Wang, C. Lv, L.-G. Niu and H.-B. Sun, *Adv. Opt. Mater.*, 2017, **5**, 1700442.
- 25 Y. Zhou, A. W. Hauser, N. P. Bende, M. G. Kuzyk and R. C. Hayward, *Adv. Funct. Mater.*, 2016, **26**, 5447–5452.
- 26 M. Li, X. Wang, B. Dong and M. Sitti, *Nat. Commun.*, 2020, **11**, 3988.
- 27 R. Luo, J. Wu, N.-D. Dinh and C.-H. Chen, *Adv. Funct. Mater.*, 2015, **25**, 7272–7279.
- 28 J. T. Robinson, S. M. Tabakman, Y. Liang, H. Wang, H. S. Casalongue, D. Vinh and H. Dai, *J. Am. Chem. Soc.*, 2011, **133**, 6825–6831.
- 29 M. Acik, G. Lee, C. Mattevi, M. Chhowalla, K. Cho and Y. J. Chabal, *Nat. Mater.*, 2010, **9**, 840–845.
- 30 D. Kim, E. Lee, H. S. Lee and J. Yoon, *Sci. Rep.*, 2015, **5**, 7646.
- 31 D. Kim, H. S. Lee and J. Yoon, *RSC Adv.*, 2014, **4**, 25379–25383.
- 32 Q. J. Yu, J. Mao, S. Wang and Z. Y. Guo, *J. Macromol. Sci., Part A: Pure Appl. Chem.*, 2020, **57**, 751–760.
- 33 H. Lin, S. Ma, B. Yu, X. Pei, M. Cai, Z. Zheng, F. Zhou and W. Liu, *Chem. Mater.*, 2019, **31**, 9504–9512.
- 34 S. Jiang, F. Liu, A. Lerch, L. Ionov and S. Agarwal, *Adv. Mater.*, 2015, **27**, 4865–4870.
- 35 L. Liu, W. Xu, Y. Ding, S. Agarwal, A. Greiner and G. Duan, *Compos. Commun.*, 2020, **22**, 100506.
- 36 L. Liu, S. Jiang, Y. Sun and S. Agarwal, *Adv. Mater.*, 2015, **26**, 1021–1027.
- 37 Z. Chen, R. Cao, S. Ye, Y. Ge, Y. Tu and X. Yang, *Sens. Actuators, B*, 2018, **255**, 2971–2978.
- 38 Z. Li, N. V. Myung and Y. Yin, *Science Robotics*, 2021, **6**, eabi4523.
- 39 G. J. Lake and A. G. Thomas, *Proc. R. Soc. A*, 1967, **300**, 108–119.
- 40 A. Buchsteiner, A. Lerf and J. Pieper, *J. Phys. Chem. B*, 2006, **110**, 22328–22338.
- 41 Y. Sun, C. Li, Y. Xu, H. Bai, Z. Yao and G. Shi, *Chem. Commun.*, 2010, **46**, 4740–4742.
- 42 J. Qi, W. Lv, G. Zhang, F. Zhang and X. Fan, *Polym. Chem.*, 2012, **3**, 621–624.
- 43 L. Zong, X. Li, X. Han, L. Lv, M. Li, J. You, X. Wu and C. Li, *ACS Appl. Mater. Interfaces*, 2017, **9**, 32280–32289.
- 44 L. Wang, Y. Jian, X. Le, W. Lu, C. Ma, J. Zhang, Y. Huang, C. F. Huang and T. Chen, *Chem. Commun.*, 2018, **54**, 1229–1232.
- 45 S. Ge, J. Li, J. Geng, S. Liu, H. Xu and Z. Gu, *Mater. Horiz.*, 2021, **8**, 1189–1198.
- 46 C. Wu and X. Wang, *Phys. Rev. Lett.*, 1998, **80**, 4092–4094.
- 47 R. Pelton, *J. Colloid Interface Sci.*, 2010, **348**, 673–674.
- 48 Z. Xu, J. Li, H. Zhou, X. Jiang, C. Yang, F. Wang, Y. Pan, N. Li, X. Li, L. Shi and X. Shi, *RSC Adv.*, 2016, **6**, 43626–43633.
- 49 J. Yan, Y. Xia, J. Lai, C. Zhao, D. Xiang, H. Li, Y. Wu, Z. Li and H. Zhou, *Macromol. Mater. Eng.*, 2022, **307**, 2100765.
- 50 Y. Liu, K. Zhang, J. Ma and G. J. Vancso, *ACS Appl. Mater. Interfaces*, 2017, **9**, 901–908.
- 51 Z. Li, J. Shen, H. Ma, X. Lu, M. Shi, N. Li and M. Ye, *Mater. Sci. Eng., C*, 2013, **33**, 1951–1957.
- 52 H. Geng, K. Zhou, J. Zhou, H. Ma, C. Lv, C. Li, Z. Xu and L. Qu, *Angew. Chem., Int. Ed.*, 2018, **57**, 15435–15440.

